HHS Public Access

Author manuscript

Mol Cancer Ther. Author manuscript; available in PMC 2017 April 01.

Published in final edited form as:

Mol Cancer Ther. 2016 April ; 15(4): 680–688. doi:10.1158/1535-7163.MCT-15-0764.

SPARC independent delivery of *nab*-paclitaxel without depleting tumor stroma in patient-derived pancreatic cancer xenografts

Harrison Kim[1,5,8], **Sharon L. Samuel**[1], **Pedro P. Lopez-Casas**[6], **William E. Grizzle**[2,5], **Manuel Hidalgo**[6], **Joy Kovar**[7], **Denise K. Oelschlager**[2], **Kurt R. Zinn**[1,5], **Jason M. Warram**[3], and **Donald J. Buchsbaum**[4,5,8]

[1]Department of Radiology, University of Alabama at Birmingham, Birmingham, Alabama 35294

[2]Department of Pathology, University of Alabama at Birmingham, Birmingham, Alabama 35294

[3]Department of Surgery, University of Alabama at Birmingham, Birmingham, Alabama 35294

[4]Department of Radiation Oncology, University of Alabama at Birmingham, Birmingham, Alabama 35294

[5]Comprehensive Cancer Center, University of Alabama at Birmingham, Birmingham, Alabama 35294

[6]Gastrointestinal Cancer Clinical Research Unit, Clinical Research Program, Spanish National Cancer Research Center, Madrid, Spain 28029

[7]LI-COR Biosciences, Lincoln, Nebraska 68504

Abstract

The study goal was to examine the relationship between *nab*-paclitaxel delivery and SPARC (secreted protein acidic and rich in cysteine) expression in pancreatic tumor xenografts and to determine the anti-stromal effect of *nab*-paclitaxel, which may affect tumor vascular perfusion. SPARC positive and negative mice bearing Panc02 tumor xenografts (n=5–6/group) were injected with IRDye 800CW (IR800)-labeled *nab*-paclitaxel. After 24 hours, tumors were collected and stained with DL650-labeled anti-SPARC antibody, and the correlation between *nab*-paclitaxel and SPARC distributions was examined. Eight groups of mice bearing either Panc039 or Panc198 patient-derived xenografts (PDXs) (4 groups/model, 5 animals/group) were untreated (served as control) or treated with gemcitabine (100 mg/kg BW, *i.p.*, twice per week), *nab*-paclitaxel (30 mg/kg BW, *i.v.*, for 5 consecutive days), and these agents in combination, respectively, for 3 weeks, and tumor volume and perfusion changes were assessed using T2-weighted magnetic resonance imaging (MRI) and dynamic contrast-enhanced (DCE) MRI, respectively. All tumors were collected and stained with Masson's Trichrome Stain, followed by a blinded comparative analysis of tumor stroma density. IR800-*nab*-paclitaxel was mainly distributed in tumor stromal tissue, but *nab*-paclitaxel and SPARC distributions were minimally correlated in either SPARC positive or negative animals. *Nab*-paclitaxel treatment did not decrease tumor stroma nor increase

[8]Requests for reprints: Hyunki Kim (; Email: Hyunki@uab.edu; phone: 205-996-4088), VH G082, University of Alabama at Birmingham, Birmingham, AL, 35294, or Donald J. Buchsbaum (; Email: djb@uab.edu; phone: 205-934-7077), WTI 630, University of Alabama at Birmingham, Birmingham, AL, 35294.

Authors do not have conflict of interest to report.

tumor vascular perfusion in either PDX model when compared to control groups. These data suggest that the specific tumor delivery of *nab*-paclitaxel is not directly related to SPARC expression, and *nab*-paclitaxel does not deplete tumor stroma in general.

Keywords

Nab-paclitaxel; SPARC; stroma; pancreatic cancer; imaging

Introduction

Pancreatic cancer is the most fatal of all common cancers, and is the fourth leading cause of cancer deaths in the United States regardless of gender. Symptoms of pancreatic cancer are non-specific, leading to diagnosis at late stages. Therefore, at diagnosis, only about 15% of patients have localized pancreatic tumors eligible for curative operations (1). For the others, various systemic therapies have been evaluated over the years. Since gemcitabine was designated as the first-line treatment in patients with advanced pancreatic cancer over a decade ago (2), a number of chemotherapies (3–8), biological therapies (9–11), and radiotherapy (12) have been tried with gemcitabine, but presented only modest clinical benefits.

Recently, the concurrent use in a clinical trial of *nab*-paclitaxel (albumin-bound paclitaxel) and gemcitabine has demonstrated better therapeutic efficacy for advanced pancreatic cancer compared to gemcitabine alone (13), and this combination has been approved by the FDA as the new first-line treatment of patients with metastatic pancreatic cancer. However, its therapeutic mechanism is not clearly understood (14). It was originally speculated that the therapeutic mechanism was associated with the interaction between *nab*-paclitaxel and SPARC (secreted protein acidic and rich in cysteine) expressed in tumor stroma (13). Since albumin binds SPARC (15) and SPARC is overexpressed in a variety of malignant tumors including pancreas adenocarcinoma (16), the effective delivery of *nab*-paclitaxel into pancreatic tumors was anticipated to be dependent upon SPARC. Of interest, the distribution pattern of human serum ablumin in tumor tissue was consistent with that of tumor stroma (17), therefore tumor uptake of *nab*-paclitaxel could be mediated by stromal SPARC. In fact, significant correlation between stromal SPARC and overall survival of patients with advanced pancreatic cancer in the phase II clinical trial of *nab*-paclitaxel plus gemcitabine was found, and *nab*-paclitaxel treatment markedly depleted tumor stroma, while significantly enhancing the tumor delivery of gemcitabine (18). In addition, a significant decrease of cancer-associated fibroblasts (CAFs) and markedly disorganized collegen were observed in residual pancreatic tumors after two cycles of *nab*-paclitaxel plus gemcitabine therapy in seven out of twelve pancreatic cancer patients (19). Therefore, it was hypothesized that *nab*-paclitaxel targets stromal SPARC to induce an antidesmoplastic effect, resulting in the increased tumoral delivery of gemcitabine when used in combination (18).

However, Neesse *et al* recently reported totally contradictory data (20), where *nab*-paclitaxel uptake into tumors was independent of SPARC expression. Tumor stroma was not depleted

after 15 days of *nab*-paclitaxel treatment at the maximum tolerable dose (60 mg/kg, q3d), and the tumor delivery of gemcitabine was not enhanced by simultaneous *nab*-paclitaxel treatment. In addition, the anti-tumor effect of *nab*-paclitaxel was not affected by the presence of stromal SPARC. SPARC independent tumor delivery and anti-tumor effect of *nab*-paclitaxel were also observed in a recent clinical study by Hidalgo *et al* (21).

The goal of the current study was to determine the relationship between *nab*-paclitaxel delivery and SPARC expression using fluorescence imaging and quantitative image analysis, and to verify whether *nab*-paclitaxel induces an anti-stromal effect and subsequent change in tumor vascular perfusion using pancreatic cancer patient-derived xenograft (PDX) mouse models.

Materials and Methods

Reagents and Cell line

All reagents were from ThermoFisher Scientific (Pittsburgh, PA) unless otherwise specified. ProHance® (gadoteridol, Bracco Diagnostics Inc., Princeton, NJ), Gemzar (gemcitabine, Eli Lilly, Indianapolis, IN) and Abraxane (*nab*-paclitaxel, Celgene, Summit, NJ) were purchased from the University of Alabama at Birmingham (UAB) Hospital Pharmacy. IRDye 800CW NHS ester was purchased from LI-COR Biosciences (Lincoln, NE). Biotinylated anti-SPARC antibody and DyLight 650-conjugated streptavidin were from Abcam (Cambridge, UK). Diamidino-2-phenylindole hydrochloride (DAPI) was purchased from Southern Biotech (Birmingham, AL). Masson's trichrome stain kit was from Polysciences, Inc (Warrington, PA). A mouse orgin pancreatic ductal adenocarcinoma cell line, Panc02, was a gift from Dr. Ignacio Melero in the University of Navarra (Pamplona, Spain) 4 years ago and was not authenticated (22).

Xenograft Establishment

Animal experiments were reviewed and approved by both the University of Alabama at Birmingham (UAB) and Spanish National Cancer Research Center (Madrid, Spain) Institutional Animal Care and Use Committee. Female athymic nude mice (6–8 weeks old; 15–20 g) purchased from Charles River Laboratories (Wilmington, MA) were used for PDX modeling. Fresh pancreatic cancer tissues were surgically removed from therapy-naïve patients, and transferred to mice at the Spanish National Cancer Research Center (Madrid, Spain) as previously described (23), and two frozen PDX tumor tissues labeled Panc039 and Panc198 were transferred to UAB. Frozen PDX tissue was thawed, and then cut into 4×4×4 mm pieces. Tumor pieces were incubated in Matrigel™ for 10 minutes, and each piece was subcutaneously inserted into the flank of each mouse. After 2–3 months, tumors were about 10 mm in diameter. For expansion, the same protocol was employed as above, but with smaller tumor pieces (2×2×2 mm). Subcutaneous tumors reached 7–8 mm in diameter in the expansion phase within 4 weeks.

SPARC positive ($SPARC^{tm1Hwe+/+}$) and SPARC-negative ($SPARC^{tm1Hwe-/-}$) mice (7 weeks old; 15–20 g; C57BL/6; female or male), purchased from The Jackson Laboratory (Bar Harbor, ME), were used to develop Panc02 tumor xenografts. Panc02 cells (1 million) were

subcutaneously injected into three female SPARC positive mice. When the tumor size was about 10 mm in diameter, tumors were collected, and a small piece of the tumor tissue (2×2×2 mm) was subcutaneously implanted into SPARC positive (n=6; three male and three female) and SPARC-negative (n=5; three male and two female) mice as described above. We assumed that stromal SPARC present in the tumor piece was ignorable.

Nab-Paclitaxel Tumor Uptake Measurement

Nab-paclitaxel was conjugated to IRDye 800CW NHS ester (LI-COR, Lincoln, NE) according to manufacturer's instructions, except less IRDye 800CW NHS ester was added in the conjugation reaction. In brief, *nab*-paclitaxel was resuspended in 1M potassium phosphate buffer (pH 8.5), and incubated with the IRDye 800CW at a D/P ratio of 0.3:1 for 2 hours at room temperature, in the dark. Following incubation, the free dye was removed from the conjugate using Pierce Zeba desalting spin columns, and the percentage of IRDye 800 attached to *nab*-paclitaxel was validated by LDS-PAGE. The IRDye 800CW to protein molar ratio was determined by measuring the absorbance of the IRDye800 labeled *nab*-paclitaxel at 280 and 780 nm, as manufacturer's instruction suggested. The molar extinction coefficients used in calculations were 38,553 $M^{-1}cm^{-1}$ and 270,000 $M^{-1}cm^{-1}$ for human serum albumin and IRDye 800CW, respectively. Female nude mice bearing either Panc039 or Panc198 tumors (n=8 per group) were *i.v.* injected with IRDye 800CW (IR800) labeled *nab*-paclitaxel (5 mg/kg BW per animal), and imaged 24 hours after injection using the Pearl® Impulse (LI-COR, Lincoln, NE), a small animal imaging system. Fluorescence light intensities in tumor and leg muscle regions were measured, and tumor-to-muscle ratio was calculated. To measure the long-term tumor-to-muscle ratio, one additional animal bearing a representative Panc039 tumor was imaged 24 times for a week after IR800-*nab*-paclitaxel injection.

When the tumor size of SPARC positive and negative mice was 7–8 mm in diameter, all mice were intravenously injected with IR800-*nab*-paclitaxel (5 mg/kg BW per animal). At 24 hours thereafter, the tumor and leg muscle tissue of each animal were collected and imaged using Pearl® Impulse. Mean fluorescence signal intensity of the tumor and muscle tissue were measured, and tumor-to-muscle ratio was calculated.

Immediately after imaging, both PDX and Panc02 tumors were fixed and processed to paraffin blocks. Tumor slices (5 μm thickness) were incubated in primary antibody (biotinylated anti-SPARC, 1:1000) in 1% bovine serum albumin in TBST overnight at 4°C. Slides were rinsed in Tris buffer three times, and secondary protein (DyLight 650 conjugated streptavidin, 1:200) was applied to the slides and incubated for 1 hour (24). DAPI staining was conducted for localizing cell nuclei. Micro-fluorescent images (0.04 × 0.03 cm) were obtained at 2–4 randomly selected areas per tumor tissue section using an Olympus IX81 Inverted Microscope (Tokyo, Japan).

In the micro-fluorescent images of PDXs, the extracellular region was determined by applying a global thresholding technique for the cell nuclear image combined with a SPARC image, when the threshold was determined based on the contrast between the cellular region and the extracellular region (25). The ratio of the total sum of IR800-*nab*-paclitaxel signal intensity in the extracellular region to that in the entire tumor region was calculated in each

image, which measures the percentage of *nab*-paclitaxel distributed in the extracellular region. In the micro-fluorescent images of Panc02 tumors, *nab*-paclitaxel and SPARC distributed regions were determined using an automatic global thresholding technique (threshold: 2 × standard deviation plus mean value of the background signal), and the ratio of the overlapping region to the *nab*-paclitaxel distributed region was calculated, which measures the correlation between *nab*-paclitaxel and SPARC distributions.

Tumor Volume and Perfusion Measurement

Four groups of mice bearing Panc039 tumors and four groups of mice bearing Panc198 tumors were used (n=5 per group). The four groups were untreated (served as control) or treated with gemcitabine (100 mg/kg BW, *i.p.*, twice per week), *nab*-paclitaxel (30 mg/kg BW, *i.v.*, for 5 consecutive days), and gemcitabine plus *nab*-paclitaxel for 3 weeks, respectively. The dose levels and dosing schedule were selected to be consistent with those of the previous study by Von Hoff *et al*, so that the results of two studies could be directly comparable (18). T2-weighted magnetic resonance imaging (T2W MRI) and dynamic contrast-enhanced magnetic resonance imaging (DCE-MRI) were applied before therapy initiation (day 0) and after completing therapy (day 21) as described in our previous studies (26, 27). T2W MRI and DCE-MRI were used to measure tumor volume and microvascular perfusion, respectively. The percentage of tumor growth inhibition (%TGI) was calculated using the equation, $\%TGI = 1-(T_f/T_i)/(C_f/C_i)$, where T_i and T_f are the tumor volumes before (day 0) and 21 days after therapy initiation, respectively. C_i and C_f are the mean tumor volumes of control animals on days 0 and 21, respectively. Wash-in rate (K^{trans}) of MR contrast in a target tissue was calculated from DCE-MR images as described in our previous study (26). Gadoteridol (Gd-HP-DO3A) was used for DCE-MRI. K^{trans} value is predominantly influenced by microvascular perfusion when a non-targeting small-molecule MR contrast agent like gadoteridol is used. After MRI on day 21, all tumors were collected and processed to paraffin blocks for histologic analysis.

Tumor Stroma Measurement

Tumor slices were stained using Masson's Trichrome Stain Kit (Polyscience, Inc, Warrington, PA). This is a three-color histology staining-kit in which fibrous tissue (e.g., collagen, reticulum) stains blue, nuclei stain purple black, and cytoplasm, muscle and erythrocytes stain red. In addition, corresponding hematoxylin and eosin (H&E) stained slides were used to evaluate the viable-appearing tumor cells. The remaining area of the slide is typically acute necrosis, most likely secondary to ischemia and/or areas of fibrin deposition. Tumor stromal tissue and viable cell densities were quantitated by a board-certified pathologist blinded to animal treatment. Digital microphotographs (X200) were taken using SPOT camera on an Olympus ix70 microscope (Tokyo, Japan), interfaced with personal computer and SPOT software.

Statistical Analysis

One-way ANOVA was used to compare the tumor volumes and K^{trans} values among the four groups untreated or treated with gemcitabine, *nab*-paclitaxel, and gemcitabine plus *nab*-paclitaxel, respectively (28). One-way ANOVA was also used to compare fluorescent imaging data or histologic findings. *P* values less than 0.05 were considered significant, after

applying Bonferroni correction for multiple comparisons (28); when p value became greater than 1 after Bonferroni correction, it was truncated to 1. Data are presented as means ±standard error. All analyses were performed with SAS, version 9.4 (SAS Institute Inc., Cary, NC).

Results

Conjugation of *nab*-paclitaxel to IRDye 800CW

The conjugation was successful with higher than 97% of the IRDye 800CW bound to *nab*-paclitaxel. The IRDye 800CW to *nab*-paclitaxel molar ratio was 0.05. This ratio indicated a single IRDye 800CW molecule was attached to 5 out of 100 *nab*-paclitaxel molecules, with 95 of 100 *nab*-paclitaxel molecules having no IRDye 800CW attached. The size of IRDye 800CW is 1.2 KDa, similar to the size of paclitaxel (0.9 KDa), and much smaller than that of *nab*-paclitaxel (66.5 KDa). Therefore, considering the low molar ratio of IRDye 800CW attached, together with the random conjugation of IRDye 800CW to any of the 60 available lysine residues in *nab*-paclitaxel, the addition of IRDye 800CW is unlikely to change the biological activity and pharmacokinetics of *nab*-paclitaxel. Previous studies demonstrated that IRDye 800CW labeled antibodies did not show differences in blood half-life compared with unlabeled antibodies, when the dye to protein (D/P) ratio was less than 2 (29, 30).

Nab-paclitaxel distribution was markedly associated with tumor stroma region

IR800-labeled *nab*-paclitaxel was accumulated preferentially in tumors in both PDX models (Fig. 1A). Tumor-to-muscle ratios in Panc039 and Panc198 tumors were 2.75±0.12 and 2.93±0.15, respectively, at 24 hours post injection, with no statistical difference between the two groups (p=0.362) (Fig. 1B). Tumor uptake of IR800-*nab*-paclitaxel was maximal at about 24 hours after injection, and the tumor-to-muscle ratio was in the range of 2–3 for six days thereafter (Fig. 1C). SPARC was expressed in both tumor stroma and tumor cells, but IR800-*nab*-paclitaxel was predominantly distributed in stroma of the tumor (Fig. 1D). Figure 2A shows the binary image of IR800-*nab*-paclitaxel shown in Fig. 1D before and after segmenting extracellular region (ECR) that was mostly tumor stroma. The ratios of the extracellular region in Panc039 and Panc198 tumors were 0.29±0.02 and 0.32±0.03, respectively (Fig. 2B). Ratios of IR800-*nab*-paclitaxel distributed in the extracellular region were 0.65±0.03 and 0.57±0.03, respectively (Fig. 2C). No statistical difference was found between the two groups (p>0.05).

Nab-paclitaxel tumor delivery was unrelated with the presence of stromal SPARC

Mean tumor size of Panc02 tumors in SPARC positive and negative animals at 21 days after implantation were 93±12 mm^2 and 97±12 mm^2, respectively, when measured using 2-dimensional fluorescent images, and no statistical difference was found between the groups (p=0.824). Tumor delivery of IR800-*nab*-paclitaxel in SPARC positive animals was comparable with that in SPARC negative animals (Fig. 3A). Tumor-to-muscle ratios in SPARC positive and negative animals were 7.83±1.43 and 10.73±1.34, respectively, without statistical difference (p=0.180) (Fig. 3B). SPARC was detected in tumors of both SPARC positive and negative animals (Fig. 3D), since Panc02 cells produce SPARC (31). SPARC expression in the tumors of SPARC positive animals was 48% higher than that of SPARC

negative animals on average, although the difference was not statistically significant (p=0.130). The correlations between *nab*-paclitaxel and SPARC distributions in the tumors of SPARC positive and negative animals were 0.10±0.02 and 0.11±0.03, respectively, without statistical difference (p=0.898) (Fig. 3C); maximum correlation would be represented with 1, and minimum would be 0.

Additive anti-tumor effect of *nab*-paclitaxel plus gemcitabine was observed

Mean tumor volumes of Panc039 and Panc198 were 230±15 mm^3 and 276±18 mm^3, respectively, prior to therapy initiation without statistical difference among the four groups in each model (p>0.05). Mean %TGI of gemcitabine, *nab*-paclitaxel, and the combination in Panc039 were 88±2%, 83±3%, and 96±1%, respectively, while those in Panc198 were 90±3%, 90±3%, and 96±2%, respectively. Mean %TGI of combination therapy in Panc039 was significantly higher than that of *nab*-paclitaxel (p=0.005), but no statistical significance was found between any other groups (p>0.05).

Nab-paclitaxel did not significantly increase microvascular perfusion in tumors

Mean K^{trans} values of Panc039 and Panc198 tumors were 0.0237±0.0009 min^{-1} and 0.0658±0.0046 min^{-1}, respectively, prior to therapy initiation (day 0) without statistical difference among the four groups in each model. Figure 4A shows representative Panc039 or Panc198 tumors untreated (control) or treated with gemcitabine, *nab*-paclitaxel, and combined agents for 3 weeks, respectively, when tumor K^{trans} maps are presented in a color scale. Figures 4B and 4C present the mean tumor volumes of Panc039 and Panc198, respectively, while Figs. 4D and 4E present the mean K^{trans} values of those, before (day 0) and 21 days after therapy initiation. Asterisks indicate statistically significant difference from the control tumors. In Panc039 tumors, mean K^{trans} value in *nab*-paclitaxel treated tumors on day 21 was larger than that in untreated tumors, but the difference was not statistically significant (p=0.699) (Fig. 4D). Of interest, mean K^{trans} value in tumors treated with gemcitabine alone or in combination with *nab*-paclitaxel was significantly higher than that in the untreated group (p=0.004 and p<0.001, respectively). Similarly, in the Panc198 model, mean K^{trans} value in *nab*-paclitaxel treated tumors was not statistically different from that in untreated tumors (p=0.316), whereas that in gemcitabine treated tumors was significantly larger than that in untreated tumors (p<0.001). However, the mean K^{trans} value in tumors receiving combination therapy was not different from untreated tumors (p=1).

Nab-paclitaxel did not decrease tumor stroma

Collagen fiber density in tumors treated with *nab*-paclitaxel for 3 weeks was significantly higher than that in untreated tumors for both Panc039 (p=0.004) and Panc198 (p=0.042) models (Fig. 5B). Of interest, Panc039 tumors treated with gemcitabine alone or in combination with *nab*-paclitaxel had significantly lower viable cell density relative to control groups (p=<0.001 and p=0.008, respectively), whereas mean viable-cell density in *nab*-paclitaxel treated tumors was not statistically different from that in control tumors in both models (p>0.05).

Discussion

In *nab*-paclitaxel treated PDX models, SPARC was expressed in both tumor stroma and tumor cells, but *nab*-paclitaxel was predominantly distributed in tumor stroma. We also demonstrated that the tumor delivery of *nab*-paclitaxel was unrelated with the presence of stromal SPARC. In addition, the *nab*-paclitaxel and SPARC distributions in a tumor were not generally coincident. Taken together, these results indicate that stromal SPARC is not the cause of the tumor specific delivery of *nab*-paclitaxel, but rather the tumor stroma itself. Since SPARC is abundant in tumor stroma and it binds albumin, it can be easily speculated that *nab*-paclitaxel targets stromal SPARC, but if so, it is hard to explain why *nab*-paclitaxel minimally interacts with SPARC expressed on tumor cells. If *nab*-paclitaxel is simply trapped in the tumor stroma, presumably because of its size, *nab*-paclitaxel will be efficiently delivered to tumors having dense stromal tissue like pancreatic adenocarcinoma; this may explain the recent success of *nab*-paclitaxel in clinical trials for advanced pancreatic cancer patients.

We also found *nab*-paclitaxel therapy did not deplete tumor stroma, consistent with the findings of Neesse *et al* (20). Von Hoff *et al*, however, showed that 4 weeks of *nab*-paclitaxel treatment markedly decreased tumor stroma in PDX models (18). This data discrepancy may be a result of the difference in cancer-associated fibroblast (CAF) sensitivity to *nab*-paclitaxel of each tumor model. Most pancreatic tumors have rich CAFs, which contribute to tumor stromal synthesis (32, 33), and dense stroma is associated with high solid stress in tumors (34). Tumor vessels commonly lack smooth muscle cells, so the accumulated tumor expansion can readily compress the tumor vessels, resulting in decreased blood perfusion and inefficient drug delivery (35). Thus, if CAFs are effectively killed by *nab*-paclitaxel, tumor stroma density is decreased, and consequently the vascular stress of tumors is reduced. This leads to relief from the compression on tumor vessels, increased blood perfusion, and in turn improved drug delivery. However, in a clinical trial, a significant decrease of CAFs was observed in only 58% of pancreatic cancer patients after *nab*-paclitaxel plus gemcitabine therapy (19). If CAFs are resistant to *nab*-paclitaxel, the tumor stroma may be only slightly affected by *nab*-paclitaxel therapy, and so would be the delivery a drug to the tumor.

Of interest, in both PDX models (Panc039 and Panc198), gemcitabine treated tumors had significantly higher microvascular perfusion than untreated tumors, while *nab*-paclitaxel treated tumors did not. Microvascular perfusion in tumors is affected not only by stromal density, but also by tumor vascularity, tumor cell density, acute necrosis density and the presence of central necrosis. Therefore, the improved perfusion after gemcitabine therapy may be associated with the increase of acute necrosis. In fact, the viable cell density in Panc039 tumors treated with gemcitabine alone or in combination with *nab*-paclitaxel was significantly lower than that in control tumors. However, it is still possible that *nab*-paclitaxel significantly increases tumor microvascular perfusion during the early therapeutic period, thus DCE-MRI at the earlier time points may be necessary to understand the microvascular change in tumors responding to *nab*-paclitaxel more accurately.

One limitation of the current study might be the fact that subcutaneous tumor xenografts do not reproduce the primary pancreatic tumor microenvironment of blood supply, neovascularization, and tumor-cell invasion. Thus the use of orthotopic PDX models that recapitulate the complexity observed in human pancreatic ductal adenocarcinoma may allow a better understanding of the therapeutic mechanism of *nab*-paclitaxel. In addition, *nab*-paclitaxel is human albumin bound paclitaxel, thus it may be questionable whether *nab*-paclitaxel interacts with mouse SPARC as effectively. However, Neesse *et al* showed that tissue and plasma concentrations of *nab*-paclitaxel were comparable with those of mouse albumin bound paclitaxel (20). Liddelow *et al* also showed that human albumin bound mouse SPARC (36).

In conclusion, our findings confirm that *nab*-paclitaxel is specifically delivered to tumor stroma in a SPARC independent manner, but *nab*-paclitaxel did not directly cause the depletion of tumor stroma or a change in tumor microvascular perfusion. Therefore the significant clinical benefits of *nab*-paclitaxel may result from its improved delivery in pancreatic cancer. Thus, development of novel drugs using albumin as a carrier would be of great interest for effective pancreatic cancer treatment (37).

Acknowledgments

Authors thank Ms. Marie Warren and Ms. Yolanda Hartman for animal modeling, animal handling, and imaging. Authors also thank Dr. Guihua Zhai for image acquisition and Mr. Camino Menendez for raising SPARC positive and negative animals. All experiments complied with current regulatory requirements (including ethics requirements) and laws of the United States of America.

Grant support: NIH grants P30CA013148 (PI: E. E. Partridge) and P50CA101955 (PI: D. J. Bucsbaum), Research Initiative Pilot Award (PI: H. Kim) from the Department of Radiology at UAB

References

1. Wray CJ, Ahmad SA, Matthews JB, Lowy AM. Surgery for pancreatic cancer: recent controversies and current practice. Gastroenterology. 2005; 128:1626–41. [PubMed: 15887155]
2. Burris HA, Moore MJ, Andersen J, Green MR, Rothenberg ML, Modiano MR, et al. Improvements in survival and clinical benefit with gemcitabine as first-line therapy for patients with advanced pancreas cancer: a randomized trial. J Clin Oncol. 1997; 15:2403–13. [PubMed: 9196156]
3. Stathis A, Moore MJ. Advanced pancreatic carcinoma: current treatment and future challenges. Nat Rev Clin Oncol. 2010; 7:163–72. [PubMed: 20101258]
4. Berlin JD, Catalano P, Thomas JP, Kugler JW, Haller DG, Benson AB. Phase III study of gemcitabine in combination with fluorouracil versus gemcitabine alone in patients with advanced pancreatic carcinoma: Eastern Cooperative Oncology Group Trial E2297. J Clin Oncol. 2002; 20:3270–5. [PubMed: 12149301]
5. Heinemann V, Quietzsch D, Gieseler F, Gonnermann M, Schönekäs H, Rost A, et al. Randomized phase III trial of gemcitabine plus cisplatin compared with gemcitabine alone in advanced pancreatic cancer. J Clin Oncol. 2006; 24:3946–52. [PubMed: 16921047]
6. Rocha Lima CM, Green MR, Rotche R, Miller WH, Jeffrey GM, Cisar LA, et al. Irinotecan plus gemcitabine results in no survival advantage compared with gemcitabine monotherapy in patients with locally advanced or metastatic pancreatic cancer despite increased tumor response rate. J Clin Oncol. 2004; 22:3776–83. [PubMed: 15365074]
7. Louvet C, Labianca R, Hammel P, Lledo G, Zampino MG, André T, et al. Gemcitabine in combination with oxaliplatin compared with gemcitabine alone in locally advanced or metastatic pancreatic cancer: results of a GERCOR and GISCAD phase III trial. J Clin Oncol. 2005; 23:3509–16. [PubMed: 15908661]

8. Abou-Alfa GK, Letourneau R, Harker G, Modiano M, Hurwitz H, Tchekmedyian NS, et al. Randomized phase III study of exatecan and gemcitabine compared with gemcitabine alone in untreated advanced pancreatic cancer. J Clin Oncol. 2006; 24:4441–7. [PubMed: 16983112]
9. Moore MJ, Goldstein D, Hamm J, Figer A, Hecht JR, Gallinger S, et al. Erlotinib plus gemcitabine compared with gemcitabine alone in patients with advanced pancreatic cancer: a phase III trial of the National Cancer Institute of Canada Clinical Trials Group. J Clin Oncol. 2007; 25:1960–6. [PubMed: 17452677]
10. Kindler HL. Pancreatic cancer: an update. Curr Oncol Rep. 2007; 9:170–6. [PubMed: 17430687]
11. Kindler HL. Front-line therapy of advanced pancreatic cancer. Semin Oncol. 2005; 32:S33–6. [PubMed: 16399428]
12. Cardenes HR, Chiorean EG, Dewitt J, Schmidt M, Loehrer P. Locally advanced pancreatic cancer: current therapeutic approach. Oncologist. 2006; 11:612–23. [PubMed: 16794240]
13. Von Hoff DD, Ervin T, Arena FP, Chiorean EG, Infante J, Moore M, et al. Increased survival in pancreatic cancer with nab-paclitaxel plus gemcitabine. The New England journal of medicine. 2013; 369:1691–703. [PubMed: 24131140]
14. Al-Batran SE, Geissler M, Seufferlein T, Oettle H. Nab-paclitaxel for metastatic pancreatic cancer: clinical outcomes and potential mechanisms of action. Oncol Res Treat. 2014; 37:128–34. [PubMed: 24685917]
15. Knauer D, Hwang L, Lowe C, Hwang J, Norng M, Trieu V, et al. Albumin-Binding and Angiogenic Domains of SPARC Located at Its C-Terminus. Cancer Res. 2009; 69:Abstract nr 2144.
16. Neuzillet C, Tijeras-Raballand A, Cros J, Faivre S, Hammel P, Raymond E. Stromal expression of SPARC in pancreatic adenocarcinoma. Cancer metastasis reviews. 2013; 32:585–602. [PubMed: 23690170]
17. Kiessling F, Fink C, Hansen M, Bock M, Sinn H, Schrenk HH, et al. Magnetic resonance imaging of nude mice with heterotransplanted high-grade squamous cell carcinomas: use of a low-loaded, covalently bound Gd-Hsa conjugate as contrast agent with high tumor affinity. Investigative radiology. 2002; 37:193–8. [PubMed: 11923641]
18. Von Hoff DD, Ramanathan RK, Borad MJ, Laheru DA, Smith LS, Wood TE, et al. Gemcitabine plus nab-paclitaxel is an active regimen in patients with advanced pancreatic cancer: a phase I/II trial. Journal of clinical oncology : official journal of the American Society of Clinical Oncology. 2011; 29:4548–54. [PubMed: 21969517]
19. Alvarez R, Musteanu M, Garcia-Garcia E, Lopez-Casas PP, Megias D, Guerra C, et al. Stromal disrupting effects of nab-paclitaxel in pancreatic cancer. British journal of cancer. 2013; 109:926–33. [PubMed: 23907428]
20. Neesse A, Frese KK, Chan DS, Bapiro TE, Howat WJ, Richards FM, et al. SPARC independent drug delivery and antitumour effects of nab-paclitaxel in genetically engineered mice. Gut. 2014; 63:974–83. [PubMed: 24067278]
21. Hidalgo M, Plaza C, Musteanu M, Illei P, Brachmann CB, Heise C, et al. SPARC Expression Did Not Predict Efficacy of nab-Paclitaxel plus Gemcitabine or Gemcitabine Alone for Metastatic Pancreatic Cancer in an Exploratory Analysis of the Phase III MPACT Trial. Clinical cancer research : an official journal of the American Association for Cancer Research. 2015; 21:4811–8. [PubMed: 26169969]
22. Corbett TH, Roberts BJ, Leopold WR, Peckham JC, Wilkoff LJ, Griswold DP Jr, et al. Induction and chemotherapeutic response of two transplantable ductal adenocarcinomas of the pancreas in C57BL/6 mice. Cancer research. 1984; 44:717–26. [PubMed: 6692374]
23. Rubio-Viqueira B, Jimeno A, Cusatis G, Zhang X, Iacobuzio-Donahue C, Karikari C, et al. An in vivo platform for translational drug development in pancreatic cancer. Clinical cancer research : an official journal of the American Association for Cancer Research. 2006; 12:4652–61. [PubMed: 16899615]
24. Green NM. Avidin. Adv Protein Chem. 1975; 29:85–133. [PubMed: 237414]
25. Dougherty, G. Digital image processing for medical applications. New York: Cambridge University Press; 2009.

26. Kim H, Samuel S, Totenhagen JW, Warren M, Sellers JC, Buchsbaum DJ. Dynamic contrast enhanced magnetic resonance imaging of an orthotopic pancreatic cancer mouse model. J Vis Exp. 2015
27. Kim H, Zhai G, Samuel SL, Rigell CJ, Umphrey HR, Rana S, et al. Dual combination therapy targeting DR5 and EMMPRIN in pancreatic adenocarcinoma. Molecular cancer therapeutics. 2012; 11:405–15. [PubMed: 22203731]
28. Neter, J.; Kutner, MH.; Nachtsheim, JC.; Wasserman, W. Applied linear statistical models. 4. Columbus: The McGraw-Hill Companies, Inc; 1996.
29. Cohen R, Stammes MA, de Roos IH, Stigter-van Walsum M, Visser GW, van Dongen GA. Inert coupling of IRDye800CW to monoclonal antibodies for clinical optical imaging of tumor targets. EJNMMI Res. 2011; 1:31. [PubMed: 22214225]
30. Zinn KR, Korb M, Samuel S, Warram JM, Dion D, Killingsworth C, et al. IND-directed safety and biodistribution study of intravenously injected cetuximab-IRDye800 in cynomolgus macaques. Molecular imaging and biology : MIB : the official publication of the Academy of Molecular Imaging. 2015; 17:49–57. [PubMed: 25080323]
31. Arnold S, Mira E, Muneer S, Korpanty G, Beck AW, Holloway SE, et al. Forced expression of MMP9 rescues the loss of angiogenesis and abrogates metastasis of pancreatic tumors triggered by the absence of host SPARC. Exp Biol Med (Maywood). 2008; 233:860–73. [PubMed: 18445772]
32. Zucker S, Hymowitz M, Rollo EE, Mann R, Conner CE, Cao J, et al. Tumorigenic potential of extracellular matrix metalloproteinase inducer. Am J Pathol. 2001; 158:1921–8. [PubMed: 11395366]
33. Seymour AB, Hruban RH, Redston M, Caldas C, Powell SM, Kinzler KW, et al. Allelotype of pancreatic adenocarcinoma. Cancer Res. 1994; 54:2761–4. [PubMed: 8168108]
34. Stylianopoulos T, Martin JD, Chauhan VP, Jain SR, Diop-Frimpong B, Bardeesy N, et al. Causes, consequences, and remedies for growth-induced solid stress in murine and human tumors. Proceedings of the National Academy of Sciences of the United States of America. 2012; 109:15101–8. [PubMed: 22932871]
35. Jain RK. Determinants of tumor blood flow: a review. Cancer research. 1988; 48:2641–58. [PubMed: 3282647]
36. Liddelow SA, Dziegielewska KM, Mollgard K, Whish SC, Noor NM, Wheaton BJ, et al. Cellular specificity of the blood-CSF barrier for albumin transfer across the choroid plexus epithelium. PLoS One. 2014; 9:e106592. [PubMed: 25211495]
37. Kratz F. Albumin as a drug carrier: design of prodrugs, drug conjugates and nanoparticles. J Control Release. 2008; 132:171–83. [PubMed: 18582981]

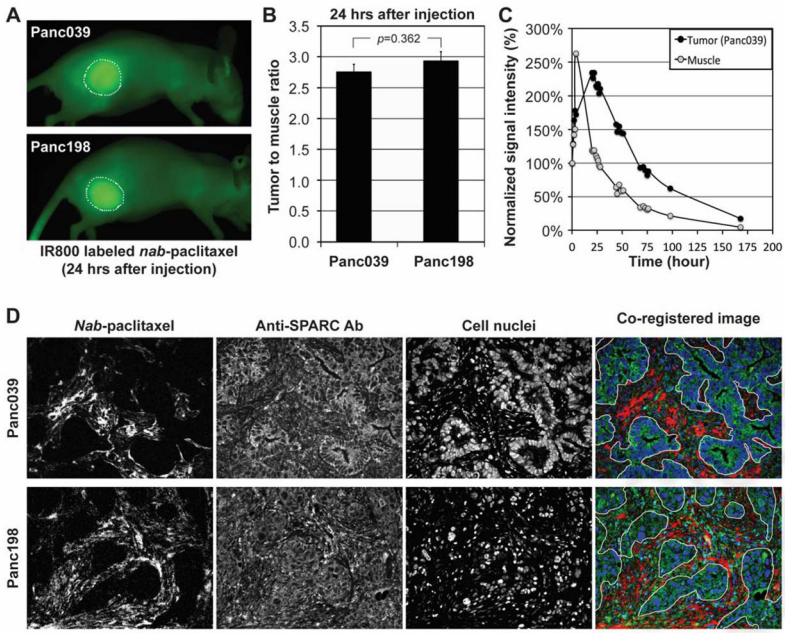

Figure 1.

In vivo and *ex vivo* optical imaging of *nab*-paclitaxel. (A) Two representative animals bearing tumor xenografts (Panc039 or Panc198) at 24 hours after injecting IR800-labeled *nab*-paclitaxel intravenously. Tumor regions are shown with dotted white circles. (B) Tumor-to-muscle ratio of fluorescent signal intensity (n=8/group) at 24 hours after intravenous IR800-*nab*-paclitaxel injection, while the error bars represent the standard error of the mean (SEM). (C) Normalized fluorescent signal intensity in the regions of tumor (Panc039) and leg muscle of a representative mouse for 7 days (168 hours). (D) Optical images of IR800-labeled *nab*-paclitaxel, DyLight 650-labeled anti-SPARC antibody, and DAPI (cell nuclear staining) with co-registered images of representative tumor tissues. In the co-registered images, IR800-labeled *nab*-paclitaxel, DyLight 650-labeled anti-SPARC antibody, and DAPI are represented with red, green and blue colors, respectively. The boundary between tumor cells and stroma is indicated with white solid lines.

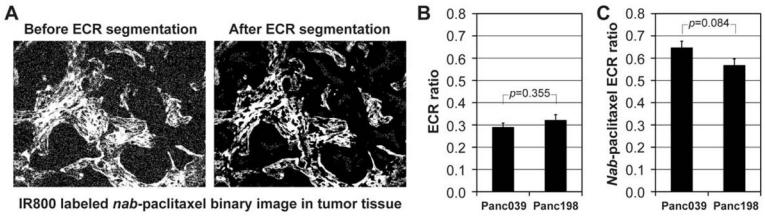

Figure 2.

Nab-paclitaxel distribution in the tumor extracellular region (ECR). (A) Binary image of IR800-labeled *nab*-paclitaxel in a Panc039 tumor xenograft (shown in Fig. 1D) before and after segmenting the extracellular region (ECR). (B) Ratio of the extracellular region to the entire tumor region in each PDX model (n=8/model). (C) Ratio of *nab*-paclitaxel distribution in the extracellular region to that in the entire tumor region in each PDX model (n=8/model). Error bars in Figs. 2B and 2C represent the standard error of the mean (SEM).

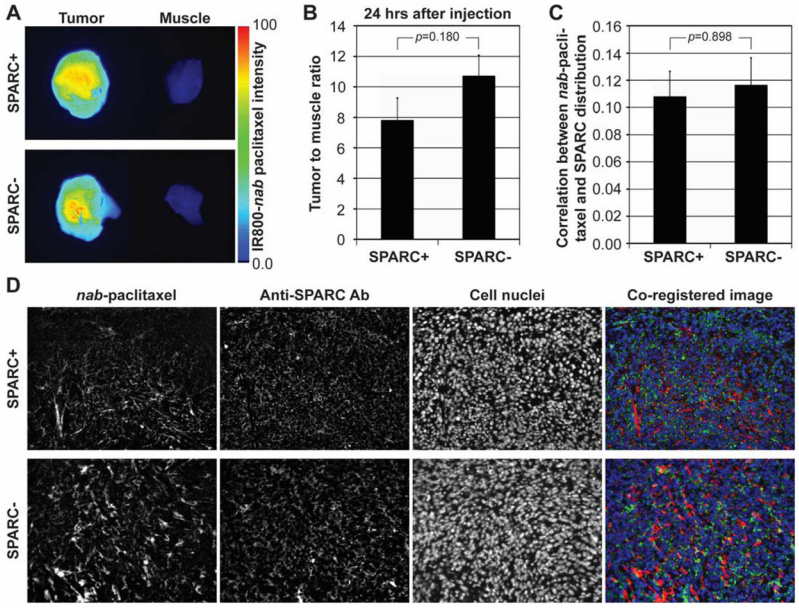

Figure 3.

Ex vivo optical imaging of *nab*-paclitaxel in Panc02 tumor xenografts of SPARC positive or negative mice. (A) *Ex vivo* optical imaging of two representative Panc02 tumors and leg muscle tissues of SPARC positive and negative mice at 24 hours after intravenous injection of IR800-labeled *nab*-paclitaxel. (B) Tumor-to-muscle ratio of fluorescence signal intensity (n=5–6/group). (C) Correlation between *nab*-paclitaxel and SPARC distributions calculated by the ratio of overlapping region to *nab*-paclitaxel distributed region. Error bars in Figs. 3B and 3C represent the standard error of the mean (SEM). (D) Optical images of IR800-labeled *nab*-paclitaxel, DyLight 650-labeled anti-SPARC antibody, and DAPI (cell nuclear staining) with co-registered images in representative Panc02 tumor tissues of SPARC positive or negative animals. In the co-registered images, IR800-labeled *nab*-paclitaxel, DyLight 650-labeled anti-SPARC antibody, and DAPI are represented with red, green and blue colors, respectively. SPARC expression was also observed in tumors of SPARC negative animals, because Panc02 cells express SPARC.

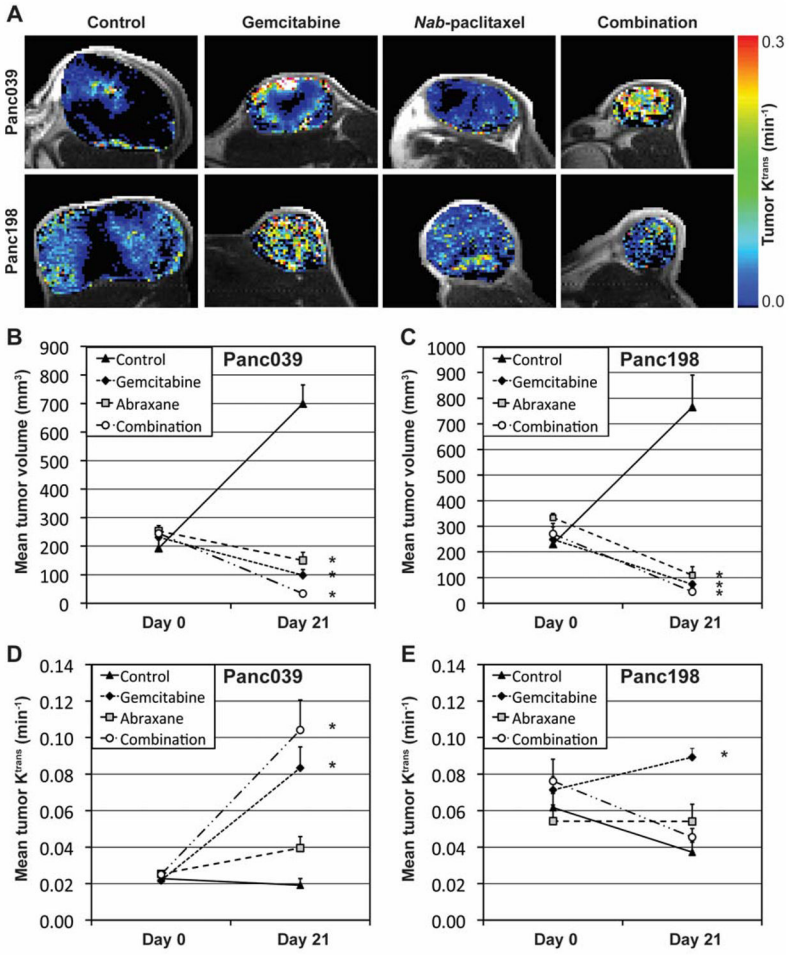

Figure 4.

Tumor volume and K^{trans} changes for 3 weeks of therapy. (A) Representative Panc039 or Panc198 tumor xenografts untreated (control) or treated with gemcitabine, *nab*-paclitaxel, and the combination for 3 weeks, respectively, while K^{trans} maps in tumor regions are shown in the color scale. (B, C) Mean tumor volumes of (B) Panc039 and (C) Panc198 before therapy (Day 0) and at 3 weeks after therapy initiation. (D, E) Mean tumor K^{trans} values of (D) Panc039 and (E) Panc198 before therapy (Day 0) and at 3 weeks after therapy initiation. Asterisk represents statistical difference from control data, and the error bars represent the standard error of the mean (SEM).

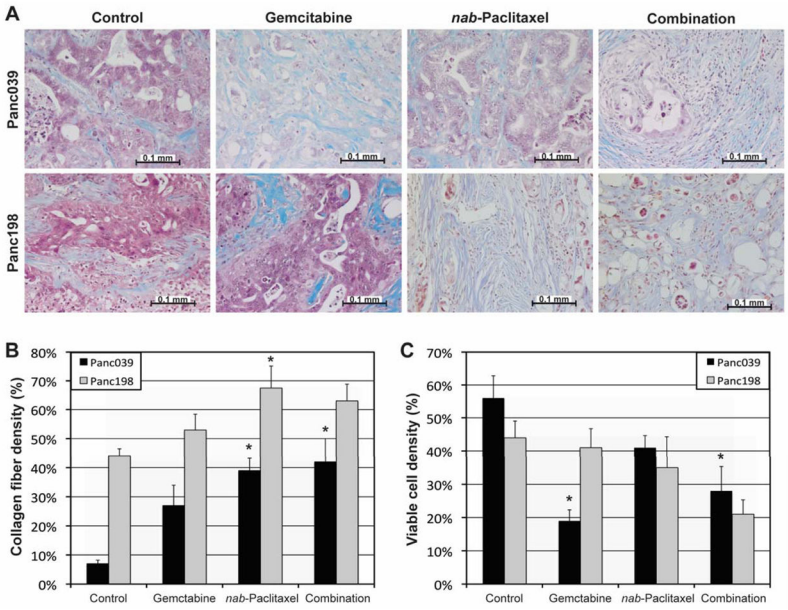

Figure 5.

Histological analyses. (A) Representative microphotographs of tumor xenografts tissues (Panc039 or Panc198) stained with Masson's Trichrome Stain, when animals were untreated (control) or treated with gemcitabine, *nab*-paclitaxel, and the combination, respectively. Collagen fibers are stained blue, nuclei stained purple black, and cytoplasm, muscle and erythrocytes are stained red. (B) Collagen fiber density. (C) Viable cell density. Asterisk represents statistical difference from control data, and the error bars represent the standard error of the mean (SEM).